

ORIGIN OF 12 μm EMISSION ACROSS GALAXY POPULATIONS FROM WISE AND SDSS SURVEYS

E. DONOSO¹, LIN YAN¹, C. TSAI¹, P. EISENHARDT², D. STERN², R. J. ASSEF^{2,6}, D. LEISAWITZ³, T. H. JARRETT⁵, S. A. STANFORD⁴

¹Spitzer Science Center, California Institute of Technology, 1200 E. California Blvd., Pasadena CA 91125, USA

²Jet Propulsion Laboratory, California Institute of Technology, Pasadena, CA 91109, USA

³Goddard Space Flight Center, Greenbelt, MD 20771, USA

⁴Department of Physics, University of California, Davis, CA 95616, USA

⁵Infrared Processing and Analysis Center, California Institute of Technology, Pasadena, CA 91125, USA and

⁶NASA Postdoctoral Program Fellow

Draft version January 17, 2012

ABSTRACT

We cross-matched Wide-field Infrared Survey Explorer (WISE) sources brighter than 1 mJy at 12 μm with the Sloan Digital Sky Survey (SDSS) galaxy spectroscopic catalog to produce a sample of $\sim 10^5$ galaxies at $\langle z \rangle = 0.08$, the largest of its kind. This sample is dominated (70%) by star-forming (SF) galaxies from the blue sequence, with total IR luminosities in the range $\sim 10^8 - 10^{12} L_{\odot}$. We identify which stellar populations are responsible for most of the 12 μm emission. We find that most ($\sim 80\%$) of the 12 μm emission in SF galaxies is produced by stellar populations younger than 0.6 Gyr. In contrast, the 12 μm emission in weak AGN ($L_{[\text{OIII}]} < 10^7 L_{\odot}$) is produced by older stars, with ages of $\sim 1 - 3$ Gyr. We find that $L_{12\mu\text{m}}$ linearly correlates with stellar mass for SF galaxies. At fixed 12 μm luminosity, weak AGN deviate toward higher masses since they tend to be hosted by massive, early-type galaxies with older stellar populations. Star-forming galaxies and weak AGN follow different $L_{12\mu\text{m}}\text{-SFR}$ (star formation rate) relations, with weak AGN showing excess 12 μm emission at low SFR ($0.02 - 1 M_{\odot} \text{yr}^{-1}$). This is likely due to dust grains heated by older stars. While the specific star formation rate (SSFR) of SF galaxies is nearly constant, the SSFR of weak AGN decreases by ~ 3 orders of magnitude, reflecting the very different star formation efficiencies between SF galaxies and massive, early-type galaxies. Stronger type II AGN in our sample ($L_{[\text{OIII}]} > 10^7 L_{\odot}$), act as an extension of massive SF galaxies, connecting the SF and weak AGN sequences. This suggests a picture where galaxies form stars normally until an AGN (possibly after a starburst episode) starts to gradually quench the SF activity. We also find that 4.6–12 μm color is a useful first-order indicator of SF activity in a galaxy when no other data are available.

Subject headings: infrared: galaxies — galaxies: active — surveys

1. INTRODUCTION

A detailed picture of the present day galaxy populations, their evolution and emission properties across different wavelengths is still far from complete. Surveys like the Sloan Digital Sky Survey (SDSS; York et al. 2000) have collected large amounts of information in the optical regime, while 2MASS (Skrutskie et al. 2006) and the IRAS mission (Neugebauer et al. 1984) have provided valuable, albeit relatively shallow, data sets from J band up to 100 μm . More recently, the Wide-field Infrared Survey Explorer (WISE; Wright et al. 2010) has completed mapping the whole sky in the mid and far infrared, at sensitivities much deeper than any other large-scale infrared survey. For example, WISE is about 100 times more sensitive at 12 μm than IRAS.

While our understanding of the optical and far-IR properties of galaxies (long-ward of 24 μm) has grown steadily, thanks mainly to Spitzer and Herschel, the spectral region between 10–15 μm remains comparatively unexplored. In normal galaxies, the light at the redder optical bands and in the J , H and K near-IR bands is closely tied to the total mass of the galaxy, as it is dominated by the red population of older stars. At wavelengths longer than $\sim 8 \mu\text{m}$, emission from dust heated by younger stars becomes increasingly relevant and begins to trace the star formation rate (SFR).

The rate at which galaxies transform gas into stars is one of the most fundamental diagnostics that describes the evolution of galaxies. Of major importance is to find what physical parameter(s) drive changes in the SFR. As dust-reprocessed light from young stars is re-emitted mainly in the far-infrared (FIR) regime, the FIR luminosity is one of the best tracers of star formation activity (Kennicutt 1998). It is well known that commonly used SFR indicators, such as the UV continuum and nebular emission line fluxes, require sometimes substantial corrections for dust extinction. Furthermore, these corrections are highly uncertain and difficult to derive. For this reason, integrated estimators based on the total infrared (IR) luminosity, either alone or in combination with the ultraviolet luminosity (e.g. Heckman et al. 1998), and monochromatic estimators based mainly on 24 μm fluxes, alone or in combination with $H\alpha$ luminosity (e.g. Wu et al. 2005; Alonso-Herrero et al. 2006; Calzetti et al. 2007; Zhu et al. 2008; Rieke et al. 2009; Kennicutt et al. 2009), are increasingly being considered as reliable star formation indicators for normal and dusty star-forming galaxies. The use of any IR flux as a SFR indicator relies on the assumption that the IR continuum emission is due to warm dust grains heated by young stars. However there is also a contribution to dust reprocessed emission by old stellar populations, associated more with the in-

terstellar medium around evolved stars than to recently born stars. In addition, some fraction of the IR luminosity may be attributed to active galactic nuclei (AGN), if present (in Section 3.8 we find AGN emission is of minor importance in most of our sample). The exact contribution of each component is difficult to estimate without detailed spectral analysis.

Chary & Elbaz (2001) and Rieke et al. (2009) found correlations between the $12\ \mu\text{m}$ luminosity and the total IR luminosity for small samples of nearby galaxies. Duc et al. (2002) found that sources in Abell 1689 with high ISO mid-IR color index $[15\ \mu\text{m}]/[6.75\ \mu\text{m}]$ are mostly blue, actively star forming galaxies, while low mid-IR flux ratios correspond to passive early-type systems. They suggest that $15\ \mu\text{m}$ emission is a reliable indicator of obscured star formation. Similarly, shorter wavelength mid-IR emission such as WISE $12\ \mu\text{m}$ is expected to be a practical tracer of star formation activity.

An important caveat is that far-infrared and/or radio measurements are only available for a small fraction of known galaxies. Early work by Spinoglio & Malkan (1989) using IRAS all-sky data used $12\ \mu\text{m}$ to select unbiased samples of active galaxies with fluxes above 220 mJy and to study their luminosity function. Deep pencil-beam surveys have complemented these samples with high redshift data. Seymour et al. (2007) conducted a $12\ \mu\text{m}$ survey of the ESO-Sculptor field (700 arcmin²) with the ISO satellite down to 0.24 mJy. Rocca-Volmerange et al. (2007) used it to model mid-IR galaxy counts, revealing a population of dusty, massive ellipticals in ultra luminous infrared galaxies (ULIRGS). Teplitz et al. (2011) performed imaging of the GOODS fields (150 arcmin²) at $16\ \mu\text{m}$ with the Spitzer spectrometer, finding that $\sim 15\%$ of objects are potentially AGN at their depth of 40-65 μJy . These surveys illustrate the necessary tradeoff between depth and area covered, potentially limiting the statistical significance of results due to cosmic variance. WISE provides the data to significantly improve the situation. Our sample of $\sim 10^5$ galaxies (see below) is over 200 times more sensitive than IRAS-based surveys and covers an area ~ 370 times larger than the GOODS samples.

In this work we explore the physical properties of $12\ \mu\text{m}$ -selected galaxies in the local Universe, using a large sample of star forming galaxies and AGN with available redshifts and emission line measurements from the SDSS. This is by far the largest $12\ \mu\text{m}$ sample to date, and we use it to trace the origin of IR emission across different galaxy populations and to investigate how IR emission relates to stellar mass. We also explore using $12\ \mu\text{m}$ luminosity as a proxy for SFR to distinguish intense starburst activity from quiescent star formation. Since we employ the SDSS spectroscopic catalog, our results apply to relatively bright galaxies at low redshift. WISE certainly recovers other populations of galaxies, ranging from low metallicity blue compact dwarf galaxies at very low redshift (Griffith et al. 2011) to highly obscured sources at high redshift (Eisenhardt et al. 2011). Lake et al. (2011) shows that WISE detects L^* galaxies out to $z \sim 0.8$ in the $3.4\ \mu\text{m}$ band, while Stern et al. (2011) shows that WISE is a very capable AGN finder, sensitive to both obscured and unobscured QSOs. A companion paper by Yan et al. (2011) analyzes more di-

verse galaxy populations observed by WISE and SDSS (including deeper photometric SDSS objects), while here we focus on $12\ \mu\text{m}$ -selected sources with available spectra.

This paper is organized as follows. In Section 2 we describe the surveys used in this work as well as explain the construction of our joint WISE-SDSS sample. In Section 3 we characterize the galaxy populations and present the results on the analysis of the mid-IR emission and SFR. Finally, Section 4 summarizes our results and discusses the implications of this work.

Throughout the paper we assume a flat Λ CDM cosmology, with $\Omega_m = 0.3$ and $\Omega_\Lambda = 0.7$. We adopt $H_0 = 70\ \text{km s}^{-1}\ \text{Mpc}^{-1}$.

2. DATA

2.1. *The Wide-field Infrared Survey Explorer Catalog*

WISE has mapped the full sky in four bands centered at 3.4, 4.6, 12 and 22 μm , achieving 5σ point source sensitivities better than 0.08, 0.11, 1 and 6 mJy, respectively. Every part of the sky has been observed typically around 10 times, except near the ecliptic poles where the coverage is much higher. Astrometric precision is better than $0.15''$ for high S/N sources (Jarrett et al. 2011) and the angular resolution is 6.1, 6.4, 6.5 and $12''$ for bands ranging from 3 μm to 22 μm .

This paper is based on data from the WISE Preliminary Release 1 (April 2011), which comprises an image atlas and a catalog of over 257 million sources from 57% of the sky. An object is included in this catalog if it: (1) is detected with $\text{SNR} \geq 7$ in at least one of the four bands, (2) is detected on at least five independent single-exposure images in at least one band, (3) has $\text{SNR} \geq 3$ in at least 40% of its single-exposure images in one or more bands, (4) is not flagged as a spurious artifact in at least one band. We refer the reader to the WISE Preliminary Release Explanatory Supplement for further details¹ (Cutri et al. 2011).

2.2. *The MPA-JHU Sloan Digital Sky Survey Catalog*

The Sloan Digital Sky Survey (York et al. 2000; Stoughton et al. 2002) is a five-band photometric (*ugriz* bands) and spectroscopic survey that has mapped a quarter of the sky, providing photometry, spectra and redshifts for about a million galaxies and quasars. The MPA-JHU catalog (Brinchmann et al. 2004, hereafter B04) is a value-added catalog based on data from the Seventh Data Release (DR7, Abazajian et al. 2009) of the SDSS². It consists of almost 10^6 galaxies with spectra reprocessed by the MPA-JHU team, for which physical properties based on detailed emission line analysis are readily available. Here we give a brief description of the catalog and the methodology employed to estimate SFRs. We refer the reader to the original papers for an in-depth discussion.

The MPA-JHU catalog classifies galaxies according to their emission lines, given the position they occupy in the BPT (Baldwin, Phillips & Terlevich 1981) diagram that plots the $[\text{OIII}]\ \lambda 5007\text{\AA}/\text{H}\beta$ versus $[\text{NII}]\ \lambda 6584\text{\AA}/\text{H}\alpha$ flux

¹ WISE data products and documentation are available at <http://irsa.ipac.caltech.edu/Missions/wise.html>

² The MPA-JHU catalog is publicly available at <http://www.mpa-garching.mpg.de/SDSS/DR7/>

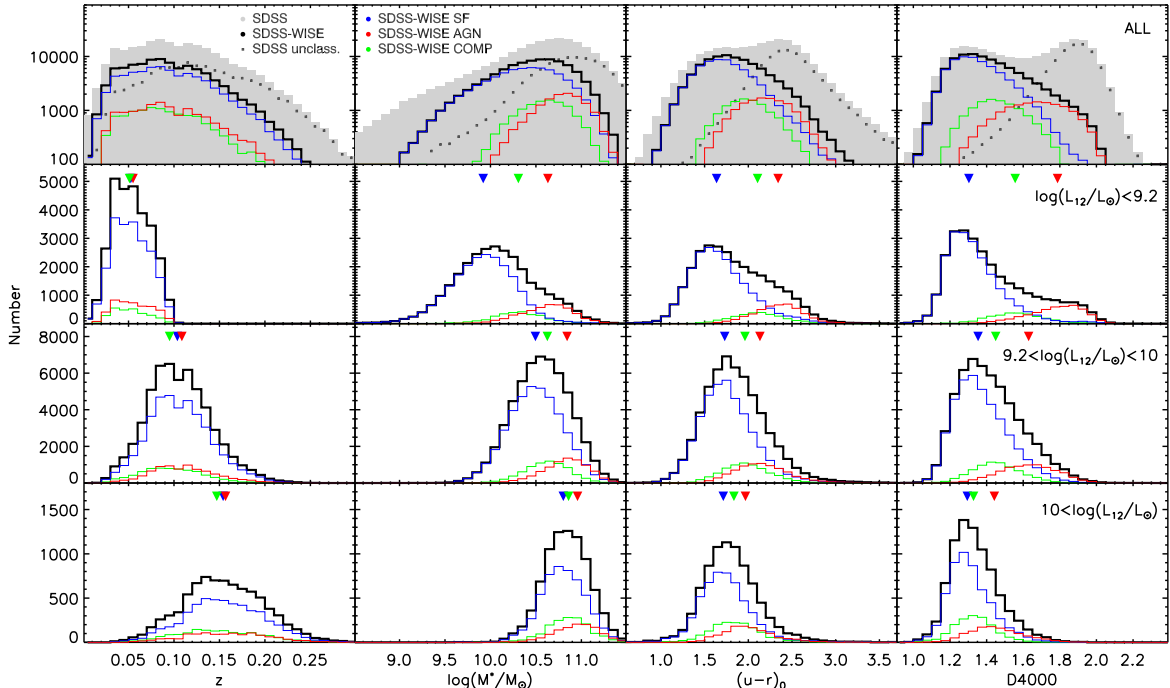


FIG. 1.— Distributions of redshift, stellar mass, restframe color $(u-r)_0$ and D_{4000} for all WISE-SDSS $12\mu\text{m}$ -selected galaxies (black), star forming galaxies (blue), AGN (red) and composite galaxies (green). We also show the distribution for all optical MPA-JHU galaxies (gray), as well as for galaxies without BPT classification due to the lack of detected emission lines (dotted). The top row shows the complete sample while the lower three rows split into low, intermediate and high IR luminosity. Triangle markers indicate the means of the respective distributions.

ratios. This separates galaxies with different ionizing sources as they populate separate sequences on the BPT diagram. In most galaxies, normal star formation can account for the flux ratios. However, in some cases an extra source such as an AGN is required. In this paper we follow this BPT classification to distinguish between: (i) **star-forming galaxies** (class SF and LOW S/N SF from B04), (ii) **active galactic nuclei** (class AGN and Low S/N LINER from B04), and (iii) **composite systems** that present signatures of the two previous types (class C from B04). Note that broad-lined AGN like quasars and Seyfert 1 galaxies are not included in the sample, as they were targeted by different criteria by the SDSS.

Star formation rates are derived by different prescriptions depending on the galaxy type. The methodology adopted by B04 is based on modeling emission lines using Bruzual & Charlot (1993) models along with the CLOUDY photoionization model (Ferland 1996) and spectral evolution models from Charlot & Bruzual (2008) to subtract the stellar continuum. To correct lines for dust attenuation, MPA-JHU adopts the multicomponent dust model of Charlot & Fall (2000), where discrete dust clouds are assumed to have finite lifetime and a realistic spatial distribution. This approach produces SFRs that take full advantage of all modeled emission lines. For AGN and composite galaxies in the sample, SFRs were estimated by the relationship between the D_{4000} spectral index and the specific SFR (SFR/M_\odot or SSFR), as calibrated for star forming galaxies (see Fig. 11 in B04). These estimates have been corrected in the latest MPA-JHU DR7 release by using improved dust attenuations and improved aperture corrections for non-SF galaxies following the work by Salim et al. (2007). Gas-phase

oxygen abundances, $12+\log(\text{O}/\text{H})$, are available for star forming galaxies as calculated by Tremonti et al. (2004). Throughout this paper we adopt the spectral line measurements as well as estimates of SFR, metallicity and dust extinction given by the MPA-JHU catalog.

The SDSS pipeline calculates several kinds of magnitudes. In this work we have adopted modified Petrosian magnitudes for flux measurements, which capture a constant fraction of the total light independent of position and distance. When appropriate, we have also used model magnitudes ($modelMag$) as they provide the most reliable estimates of galaxy colors. Magnitudes are corrected for galactic reddening using the dust maps of Schlegel, Finkbeiner & Davis (1998).

2.3. The Joint WISE-SDSS Galaxy Sample

We have crossmatched data from WISE and the MPA-JHU catalog to construct a galaxy sample covering an effective area of 2344 deg^2 , or 29% of the DR7 (legacy) spectroscopic footprint. WISE sources were selected to have $12\mu\text{m}$ fluxes above 1 mJy, also requiring objects to have clean photometry at 3.4, 4.6 and $12\mu\text{m}$. For MPA-JHU sources, we selected objects with de-reddened Petrosian magnitude $r_{\text{petro}} < 17.7$ and r -band surface brightness $\mu_r < 23\text{ mag arcsec}^{-2}$. This selects a conservative version of the SDSS main galaxy sample (see Strauss et al. 2002). Using a matching radius of $3''$ we find 96,217 WISE objects with single optical matches (40% of the SDSS sample in the intersection area), and 73 sources with two or more counterparts. The latter are mostly large extended sources or close interacting systems of two members. For the rest of this paper we will focus on the single IR-optical matches that constitute the vast majority (>99.9%) of the galaxy population. By us-

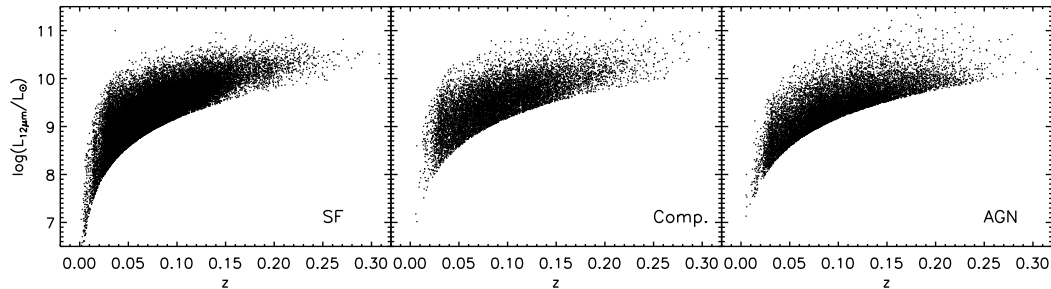


FIG. 2.— Distribution of $12\ \mu\text{m}$ luminosity for galaxies separated according to spectral type as: SF galaxies (left), composite systems (middle), and AGN (right).

ing random catalogs generated over the effective area, the expected false detection fraction at $3''$ is 0.05%.

Each region of the sky has been observed at least 10 times by WISE, with the number of observations increasing substantially toward the ecliptic poles. Within our effective area, the median coverage depth at $12\ \mu\text{m}$ is about 13, varying typically between 10 and 20. At these levels, the average completeness of the sample is expected to be over 90%, as shown in the WISE Preliminary Release Explanatory Supplement (Sec. 6.6).

3. ANALYSIS AND RESULTS

3.1. Derived Properties

We derived stellar masses for all galaxies using the *kcorrect* algorithm (Blanton & Roweis 2007), which fits a linear combination of spectral templates to the flux measurements for each galaxy. These templates are based on a set of Bruzual & Charlot (2003) models that span a wide range of star formation histories, metallicities and dust extinction. This algorithm yields stellar masses that differ by less than 0.1 dex on average from estimates using other methods (for example, the method based on fitting the 4000\AA break strength and $H\delta$ absorption index proposed by Kauffmann et al. 2003a).

To derive restframe colors and monochromatic luminosities in the infrared we used the fitting code and templates³ of Assef et al. (2010), applied to our combined *ugriz* photometry plus WISE $3.4\ \mu\text{m}$, $4.6\ \mu\text{m}$ and $12\ \mu\text{m}$ fluxes. Assef et al. (2010) present a set of low-resolution empirical spectral energy distribution (SED) templates for galaxies and AGN spanning the wavelength range from $0.03\ \mu\text{m}$ to $30\ \mu\text{m}$, constructed with data from the NOAO Deep Wide-Field Survey Boötes field (NDFWS, Jannuzi et al. 2010) and the AGN and Galaxy Evolution Survey (AGES, Kochanek et al. 2011). The code fits three galaxy SED templates that represent an old stellar population (elliptical), a continuously star-forming population (spiral) and a starburst component (irregular), plus an AGN SED template with variable reddening and IGM absorption. These templates have been successfully used to test the reliability of IRAC AGN selection, and to predict the color-color distribution of WISE sources (Assef et al. (2010)). We also use these templates to assess the relative contribution of AGN to the energy budget.

Instead of trying to derive a new calibration of the SFR in the IR, we take the approach of comparing IR luminosities directly to optical dust-corrected SFRs. This makes our results largely independent of any particular

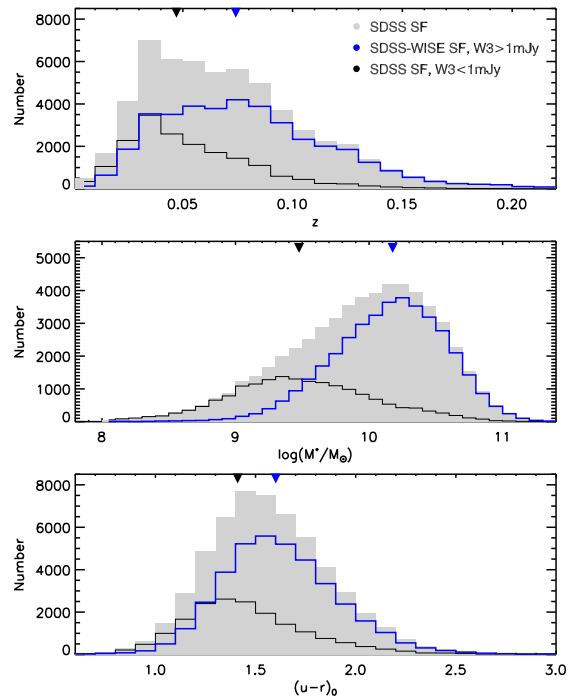


FIG. 3.— Distribution of redshift, stellar mass and restframe color $(u-r)_0$ for WISE-SDSS $12\ \mu\text{m}$ -selected galaxies classified as star forming (blue). We also show the distributions for all optical star-forming galaxies (gray) and for star-forming galaxies without $12\ \mu\text{m}$ flux densities above 1 mJy (black). Triangle markers indicate the means of the distributions.

SFR calibration. Note all optical SFRs used in this paper have been corrected for dust extinction.

3.2. General Properties of $12\ \mu\text{m}$ Galaxies

We begin our analysis by exploring the general properties of the WISE $12\ \mu\text{m}$ -selected galaxy sample. The sample is composed of a mixture of 70% SF galaxies, 15% AGN, 12% composite galaxies and 3% galaxies lacking BPT classification due to the absence of detectable lines in the spectra (most lack $H\alpha$ emission). The composition of the MPA-JHU optical sample is 44% SF, 12% AGN, 6% composite, 37% unclassifiable, which means that the $12\ \mu\text{m}$ selection is highly efficient in recovering SF systems and avoids objects with weak or no emission lines. In terms of the total optical galaxy populations, 61% (SF), 53% (AGN) and 76% (composite) of the SDSS galaxies have $12\ \mu\text{m}$ flux densities above 1 mJy. In Figure 1 (top row) we plot the distribution of redshift, stellar mass, D_{4000} index and restframe $u-r$ color for SF galaxies, AGN and composite systems, as well as for the three classes all together. The majority of WISE-SDSS

³ Templates and code are available at <http://www.astronomy.ohio-state.edu/~rjassef/lrt/>

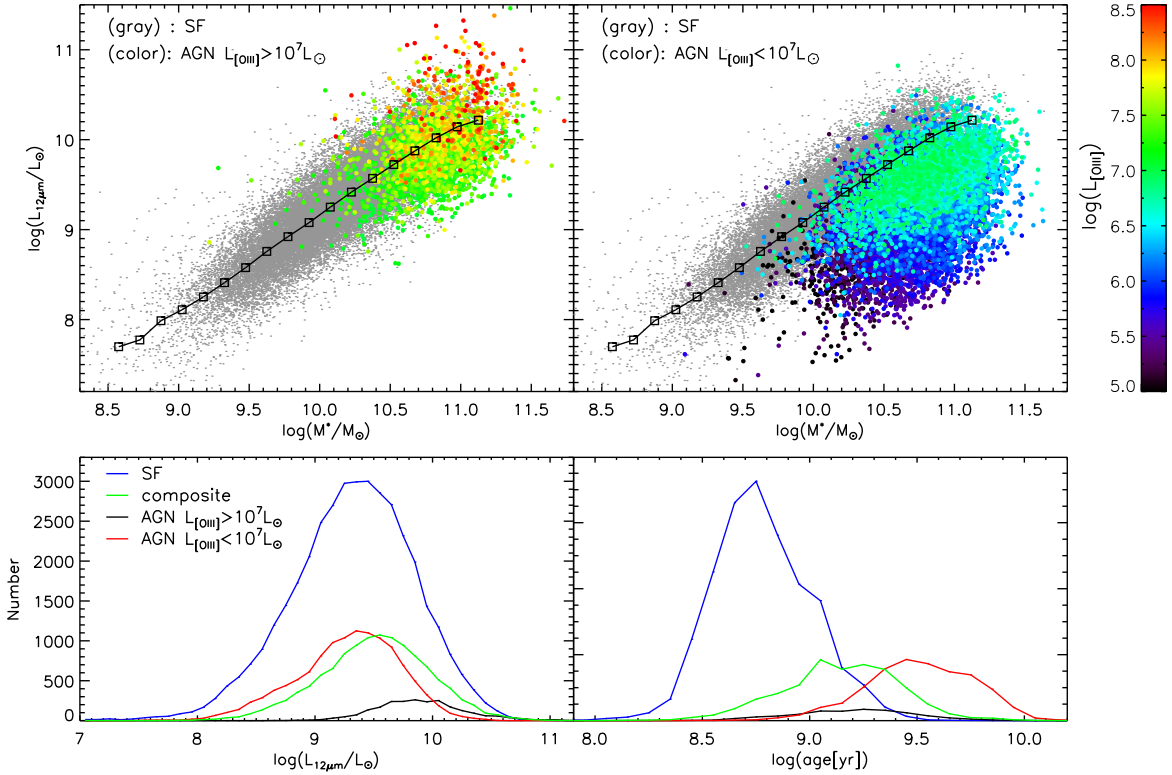


FIG. 4.— $12\mu\text{m}$ infrared luminosity as a function of stellar mass for SF galaxies (gray), strong AGN with $L_{[\text{OIII}]} > 10^7 L_\odot$ (color points, top left), and weak AGN with $L_{[\text{OIII}]} < 10^7 L_\odot$ (color points, top right). The solid line shows the median $L_{12\mu\text{m}}$ of SF galaxies as a function of mass. Bottom panels show the distribution of $L_{12\mu\text{m}}$ and stellar age for the various populations as indicated.

$12\mu\text{m}$ sources are SF galaxies at $\langle z \rangle = 0.08$ with stellar masses of $\sim 10^{10.2} M_\odot$; these are typical values for the SF class. They clearly populate the blue peak of the galaxy bimodal distribution around $(u-r)_0 = 1.6$ and have inherently young stellar populations ($D_{4000} \sim 1.3$, or ages of ~ 0.5 Gyr). AGN are, as expected, comparatively more massive ($M^* \sim 10^{10.7} M_\odot$), redder ($(u-r)_0 \sim 2.1$) and older ($\sim 1-6$ Gyr), dominating the massive end of the $12\mu\text{m}$ galaxy distribution. As a population, AGN do not differ significantly (in terms of these properties) in comparison to the corresponding purely optical sample. Composite galaxies present intermediate properties between the SF and AGN samples. Note that the bulk of galaxies lacking BPT classification (due to weak or absent emission lines) is missed in our IR-optical sample. These objects primarily populate the red sequence of the galaxy distribution (e.g. Baldry et al. 2004) and hence are not expected to be prominent at $12\mu\text{m}$.

We then divide the sample into three subsamples of monochromatic infrared luminosity: faint ($L_{12\mu\text{m}} < 10^{9.2} L_\odot$), intermediate ($10^{9.2} L_\odot < L_{12\mu\text{m}} < 10^{10} L_\odot$), and bright ($L_{12\mu\text{m}} > 10^{10} L_\odot$) sources. There are no large biases with redshift, i.e. the different classes are sampled roughly without preference at all luminosities. Both SF galaxies and AGN become more massive for higher IR luminosities and we have checked that this also holds in narrow redshift slices. As we will show below, this is due to the coupling between the IR and the optical emission. Interestingly, the $12\mu\text{m}$ SF galaxies change by a factor of 0.8 dex in mass toward high $12\mu\text{m}$ luminosities while keeping the same color and stellar content. The AGN population, while getting slightly more massive, becomes

bluer and dominated by younger stars as IR luminosity increases. Figure 2 shows the redshift distribution of the restframe $12\mu\text{m}$ luminosity for our sample. It can be seen that while high luminosity sources naturally lie at higher redshifts, the redshift distribution of the different classes is very similar, except at the lowest redshifts ($z < 0.02$) where very few AGN/composite galaxies are observed.

The absence of red sequence galaxies in our sample is not surprising, but there is also a number of SF galaxies without IR emission due to our flux limit. Figure 3 shows the mass, redshift and colors of SF galaxies with and without $12\mu\text{m}$ emission, as well as for the entire SF optical sample. On average, SF galaxies not present in our sample have bluer colors, lie at lower redshifts, and have stellar masses around $10^{9.3} M_\odot$, roughly an order of magnitude below the $12\mu\text{m}$ SF galaxy sample. At this level, galaxies have very little dust mass, and hence can not re-radiate much in the IR.

The main result here is that WISE $12\mu\text{m}$ -selected galaxies are primarily typical blue sequence (SF) galaxies. It is safe to assume that the majority of blue sequence galaxies correspond to late morphological types (e.g. Strateva et al. 2001; Shimasaku et al. 2001; Baldry et al. 2004). AGN and composite objects are also represented, belonging either to the red sequence or to a transitional regime among the two former classes. It is interesting that the detection efficiency is largest for composite systems, which was also found by Salim et al. (2009) for $24\mu\text{m}$ sources that lie in the so called *green valley* (e.g. Martin et al. 2007). This is a region located between the red and blue cloud sequences, best identified

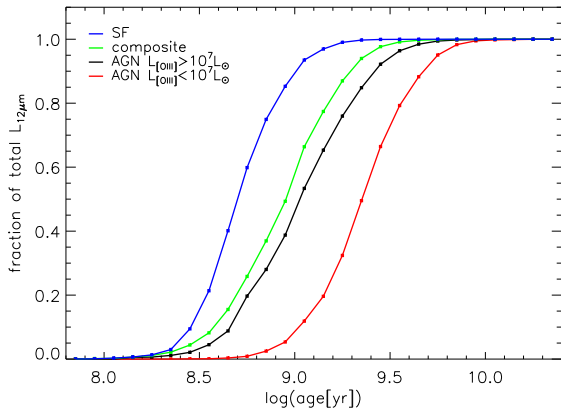


FIG. 5.— Cumulative fraction of integrated $12\mu\text{m}$ luminosity for galaxies dominated by stellar populations of a given age, separated according to spectral type as: SF galaxies (blue), composite systems (green), strong AGN (black) weak AGN (red).

in the NUV- r color-magnitude diagram, where SF activity is being actively quenched and galaxies are thought to be in transitional stage in their migration from the blue to the red sequence.

Most galaxies in our sample are either normal luminosity IR galaxies ($L_{12\mu\text{m}} \sim 10^{9.2-10} L_{\odot}$; 60%), low luminosity IR galaxies ($L_{12\mu\text{m}} < 10^{9.2} L_{\odot}$; 31%) or luminous infrared galaxies (LIRGs; $L_{12\mu\text{m}} \sim 10^{10-10.8} L_{\odot}$; 9%). However, ULIRGs are also present. There are 114 objects with $L_{12\mu\text{m}} > 10^{10.8} L_{\odot}$ (roughly equivalent to $L_{\text{TIR}} > 10^{12} L_{\odot}$ using the conversion of Chary & Elbaz 2001), corresponding to a surface density of 0.049 deg^{-2} . This is comparable to the 0.041 deg^{-2} surface density found by Hou, Wu & Han (2009). These ULIRGs naturally lie at higher redshift ($z = 0.2$) and populate the massive end of the SF sequence above $\sim 10^{11} M_{\odot}$. We reiterate that these results come from matching WISE to the relatively bright SDSS spectroscopic sample. WISE galaxy populations down to $r \sim 22.6$ are analyzed in Yan et al. (2011).

3.3. $12\mu\text{m}$ Luminosity and Stellar Mass

We now have a large sample of $12\mu\text{m}$ -selected galaxies that range from low-IR to ULIRG luminosities, for which high quality optical spectra and dust-corrected optical SFRs are available. First we examine the relation between $L_{12\mu\text{m}}$ and stellar mass. B04 have shown that, at least for star forming systems, SFR and stellar mass are strongly correlated in the local universe. There is also evidence that this relationship evolves with redshift (Noeske et al. 2007, Daddi et al. 2007). Although it is expected that more massive galaxies are naturally more luminous, it is unclear whether more massive systems would have more dust emission in the mid-IR. Figure 4 shows the correlation between monochromatic $12\mu\text{m}$ luminosity and stellar mass for our sample. The correlation is tight for SF systems over nearly three orders of magnitude in stellar mass (gray points, top panels). Several studies have found that the distributions of [OIII] emission line flux to the AGN continuum flux at X-ray, mid/far-IR and radio wavelengths (i.e. where stellar emission and absorption by the torus are least significant) are very similar for both type I and type II AGN (Mulchaey et al. 1994; Keel et al. 1994; Alonso-Herrero et al. 1997). Based on this, Kauffmann et al. (2003b) and

Heckman et al. (2004) have shown that [OIII] flux is a reliable estimator of AGN activity. Following these works, we split the AGN sample by [OIII] luminosity. We see that strong AGN ($L_{[\text{OIII}]} > 10^7 L_{\odot}$) have IR luminosities considerably larger than weak AGN ($L_{[\text{OIII}]} < 10^7 L_{\odot}$), following approximately the same relationship with mass as SF systems. Weak AGN, instead, lie well below that correlation and show a larger scatter. We note that the contribution by star forming regions to the [OIII] flux is $< 7\%$ (Kauffmann et al. 2003b).

In the right bottom panel of Figure 4 we compare the ages of stars in all subsamples as derived from the D_{4000} spectral index. SF galaxies have the youngest stellar populations, peaking at ~ 0.5 Gyr, followed by considerably older composite galaxies ($\sim 1.5-2$ Gyr). Strong AGN, which dominate the massive end, have intermediate stellar populations (~ 1.5 Gyr) that are closer to SF/Composite systems than to weak AGN (see Fig. 1). In contrast, weak AGN tend to be hosted by early-type galaxies with significantly older stars (~ 3 Gyr) as found also by Kauffmann et al. (2003b) after comparing AGN host sizes, surface densities and concentration ratios with those of normal early-type galaxies. This highlights the importance that young/old stars have in powering the $12\mu\text{m}$ emission. For AGN of roughly similar stellar mass, only when younger stars begin to dominate (and the active nuclei becomes more powerful) is the IR emission comparable to actively star-forming systems. Qualitatively, the same result holds if we use the dust-corrected r -band absolute magnitude instead of stellar mass.

Since galaxies of different ages have very different IR output, an interesting question to address is how the $12\mu\text{m}$ luminosity budget depends upon the age of the stellar populations. Figure 5 shows the cumulative fraction of the *integrated* $12\mu\text{m}$ luminosity produced in galaxies of a given age. In SF galaxies, $\sim 80\%$ of the total IR luminosity is produced by galaxies younger than 0.6 Gyr. Composite galaxies and strong AGN reach the same fraction at ages of 1.5 Gyr and 2 Gyr, respectively. In weak AGN, instead, most of the mid-IR emission is produced within a range of $\sim 1-3$ Gyr. This inventory of $12\mu\text{m}$ luminosity in the local universe shows where the bulk of the IR emission resides, shifting from stellar populations of a few hundred Myr in actively SF galaxies to a few Gyr in galaxies hosting weak AGN. Thus, it underlines again the important role that young/old stars have in powering $12\mu\text{m}$ emission. As we will see later in Section 3.6, this also supports the idea that transition galaxies (i.e. composite/strong AGN) form a smooth sequence that joins highly active galaxies with quiescent galaxies.

3.4. $12\mu\text{m}$ Luminosity and Star Formation Rate

We now explore the relationship between infrared luminosity and optical, dust-corrected SFR. Figure 6 shows $L_{12\mu\text{m}}$ versus SFR_{opt} , color-coded by the D_{4000} spectral index. As discussed by Kauffmann et al. (2003a), the D_{4000} index is a good indicator of the mean age of the stellar population in a galaxy. The dashed line indicates the reference relation of Kennicutt (1998), as given by Chary & Elbaz (2001) in terms of $12\mu\text{m}$ luminosity, to convert IR luminosity into “instantaneous” SFR. It was derived from simple theoretical models of stellar popula-

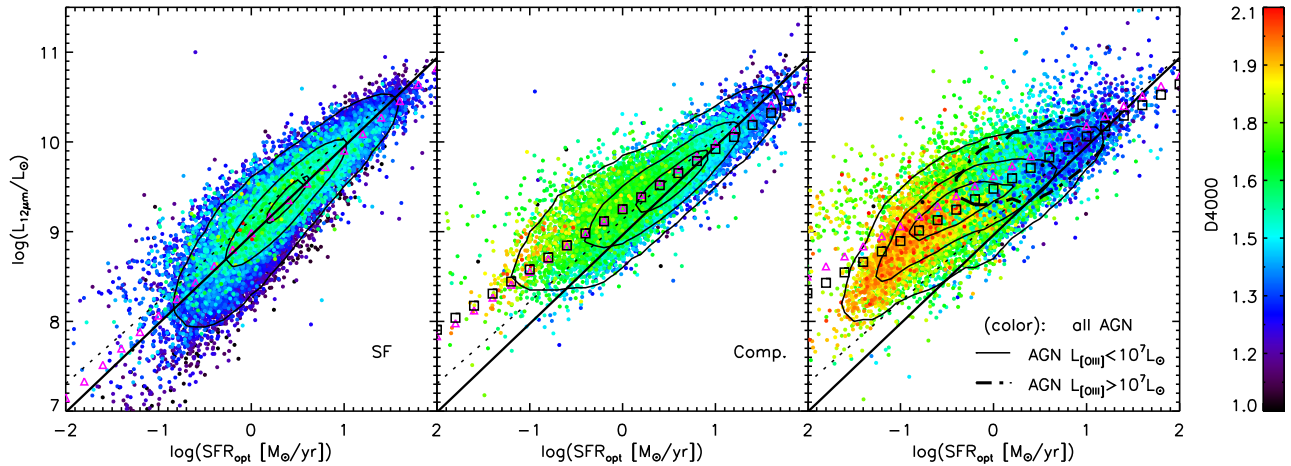


FIG. 6.— Infrared luminosity at $12\ \mu\text{m}$ as a function of dust-corrected star formation rate derived from optical emission lines, for galaxies classified as SF (left), Composite (middle) and strong/weak AGN (right). Linear fits are shown for the cases of: SF galaxies (solid line, all panels), composite systems (squares, middle panel) and AGN (squares, right panel). The dashed line is the Chary & Elbaz (2001) conversion between SFR and $12\ \mu\text{m}$ luminosity. For sources brighter than 5 mJy at $22\ \mu\text{m}$, we also plot the corresponding $L_{22\ \mu\text{m}}$ –SFR relationships (triangles). In all panels, the mean stellar age of the dominant stellar population is indicated by the D_{4000} color scale on the right. Contours enclose 95%, 68% and 33% of the density distribution (68% for the case of strong AGN).

tions with ages 10–100 Myr without considering factors like metallicity or more complex star formation histories. While this makes it strictly valid only for young starbursts, the Kennicutt relation is quite often applied to the more general population of star forming galaxies. Figure 6 shows that the IR emission from SF galaxies (left panel) correlates fairly well with SFR_{opt} . The correlation is tighter for high SFRs becoming broader and slightly asymmetric for low SFRs. A least-squares fit to the SF sample is given by

$$\log L_{12\ \mu\text{m}}^{\text{SF}} = (0.987 \pm 0.002) \log SFR_{\text{opt}} + (8.962 \pm 0.003). \quad (1)$$

This expression is close to the Chary & Elbaz (2001) relation at high SFRs, which is not surprising given that relation was calibrated using the IRAS Bright Galaxy Sample (Soifer et al. 1987), i.e. luminous galaxies with $L_{12\ \mu\text{m}} > 10^9 L_{\odot}$. The small differences are likely attributable to luminosity/redshift selection effects and the slight differences between ISO and WISE $12\ \mu\text{m}$ filters. More importantly, the agreement is quite good considering the different origin (FIR vs optical emission lines) of the SFRs. Relative to the Chary & Elbaz (2001) conversion, $L_{12\ \mu\text{m}}$ is comparatively suppressed by a factor > 1.6 for SFR_{opt} below $\sim 0.1 M_{\odot} \text{yr}^{-1}$. This is likely because low SFR systems have very low stellar masses ($< 10^9 M_{\odot}$), and therefore become more transparent due to the increasing fraction of stellar light that escapes unabsorbed by dust. We note, however, that the spatial distribution of dust in HII regions and/or molecular clouds could also have influence (e.g. Leisawitz & Hauser 1988). In addition, we have repeated the test for the bluest galaxies in the SF galaxy class, obtaining no significant differences. This suggests that other effects like metallicity could also be relevant.

For AGN, the coupling between optical SFR and IR luminosity follows a different relationship (right panel of Figure 6). Most AGN lie in a broader distribution *above* the instantaneous conversion of Kennicutt, particularly those with SFR_{opt} below $\sim 1 M_{\odot} \text{yr}^{-1}$. For a fixed SFR, the IR emission is higher by a factor of several relative to SF galaxies, suggesting that $L_{12\ \mu\text{m}}$ is not

driven by the current SF for most AGN. Weak AGN are predominantly associated with massive, early-type galaxies increasingly dominated by old stars at low SFRs ($\sim 0.1 M_{\odot} \text{yr}^{-1}$). Given their red optical colors, it is unlikely that recent SF could be responsible for their IR emission. More likely, dust grains heated due to older stars or an AGN are driving this emission. Note, however, that in Section 3.8 we will show that the contribution of AGN at $12\ \mu\text{m}$ is of minor importance for most AGN, except perhaps for most powerful ones. Only strong AGN, which are dominated by intermediate-to-young stellar populations, tend to occupy a region similar to SF galaxies in Figure 6. They show a clear “excess” in $L_{12\ \mu\text{m}}$ at $SFR_{\text{opt}} \sim 0.5 M_{\odot} \text{yr}^{-1}$ that gradually decreases when stars get younger toward higher SFRs. This shows that the age of stars in an AGN is an important factor in determining the origin of the $12\ \mu\text{m}$ emission. An expression fitting AGN (weak and strong) is given by

$$\log L_{12\ \mu\text{m}}^{\text{AGN}} = (0.582 \pm 0.004) \log SFR_{\text{opt}} + (9.477 \pm 0.002). \quad (2)$$

Recent work by Salim et al. (2009) compared NUV/optical SFRs with L_{TIR} calibrated from $24\ \mu\text{m}$ fluxes for red and green sequence objects at $z \sim 0.7$ (corresponding to restframe $14\ \mu\text{m}$, close to the WISE $12\ \mu\text{m}$ band). They find large excess IR emission for a given SFR, attributed mainly to older stellar populations, and to a lesser extent to an AGN. We find broadly consistent results, but for $12\ \mu\text{m}$ -selected AGN sources with optical SFRs. Kelson & Holden (2010) have suggested that thermally pulsating AGB carbon stars (TP-AGB) with ages of 0.2–1.5 Gyr (corresponding to $D_{4000} \sim 1.2$ –1.5) can also contribute significantly to the mid-IR flux. As seen in Section 3.3, this does not seem to be important for our much older, weak AGN, and perhaps marginally relevant in strong AGN that have typical stellar ages slightly above the upper 1.5 Gyr limit. The case of SF galaxies is interesting because most of the $12\ \mu\text{m}$ luminosity seems to originate from galaxies in the ~ 0.3 –0.6 Gyr age range and this luminosity correlates relatively well with the optical SFR. While the age ranges seems to overlap, it is difficult to prove whether TP-AGB dominate the emis-

sion or not. Further SED decomposition and modeling of stellar populations is required to find the fraction of mid-IR luminosity powered by TP-AGB stars, a task that is potentially complicated by metallicity effects and uncertainties in the ensemble colors of such stars. However, the general picture is consistent with previous results (Salim et al. 2009; Kelson & Holden 2010) that find evidence for the mid-IR being sensitive to star formation over relatively long (>1.5 Gyr) timescales.

Finally, we consider composite systems, which present considerable SF activity along with spectral signatures of an AGN (middle panel of Figure 6). By definition, these objects have up to 40% (see B04) of their $H\alpha$ emission coming from a non-stellar origin, though the fraction is $<15\%$ for most galaxies. With masses, ages and optical colors intermediate between the SF and AGN sequences, composite galaxies closely follow the Kennicutt relation, except at the low SFR end where older stars once again begin to dominate. A least-squares fit for composite galaxies has a slope intermediate between AGN and SF galaxies, and is given by

$$\log L_{12\mu\text{m}}^{\text{comp}} = (0.671 \pm 0.003) \log SFR_{\text{opt}} + (9.249 \pm 0.002). \quad (3)$$

We note that the optical SFRs utilized here, while not ideal, are probably the best estimates publicly available for such a large and diverse population of galaxies in the local universe. Other methodologies that use more sophisticated dust corrections and employ H_2 , FIR or radio data could provide more accurate values, but are difficult to apply across the entire sample and data are not always available (see Saintonge et al. 2011 for a calibration of SFR based on H_2 masses). This is particularly relevant for SFRs in AGN, which can present large >0.5 dex formal errors (see Figure 14 of Brinchmann et al. 2004). We have verified that the SDSS SFRs in our sample are in broad agreement with UV-based SFRs derived by Salim et al. (2007) (S. Salim, private communication), with an average offset/scatter of 0.055/0.387 for the total sample (0.013/0.334 for strong AGN, 0.242/0.567 for weak AGN).

3.5. $22 \mu\text{m}$ Luminosity and Star Formation Rate

WISE is less sensitive at $22 \mu\text{m}$ than at $12 \mu\text{m}$, but a significant fraction of our sample ($\sim 30\%$) has measured $22 \mu\text{m}$ fluxes above 5 mJy (note we find no $22 \mu\text{m}$ galaxies without $12 \mu\text{m}$ detection). Similar to the $12 \mu\text{m}$ sample, this $22 \mu\text{m}$ subsample is a mixture comprised of 65% SF galaxies, 14% AGN and 19% composite systems. However, the fraction of strong AGN is 38%, compared to 16% for $12 \mu\text{m}$ sources. As $22 \mu\text{m}$ is closer to the dust emission peak and is not affected by PAH emission features, it is interesting to compare with the $12 \mu\text{m}$ galaxies of our previous analysis. Figure 6 shows the linear fits for the $22 \mu\text{m}$ subsample (triangle markers). These relations are very similar to the $12 \mu\text{m}$ fits (solid line for SF galaxies, square markers for AGN and composite galaxies), supporting the independence of our results on the particularities of a single mid-IR band.

3.6. Specific Star Formation Rate

Given the strong correlations between optical or IR light and stellar mass, a more interesting metric for comparison is the specific star formation rate, SSFR or

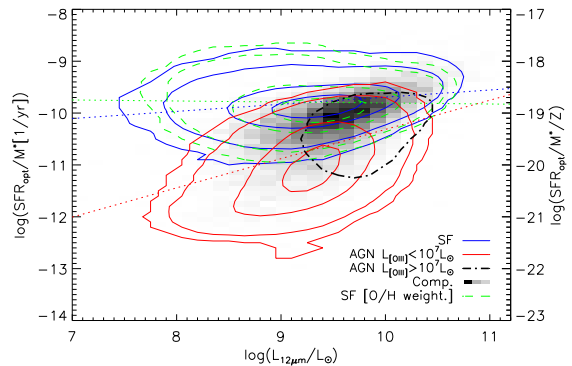


FIG. 7.— Specific star formation rate (SSFR) as a function of $12 \mu\text{m}$ luminosity for SF galaxies (blue), AGN (red), and composite galaxies (grayscale). The metallicity-weighted SSFR for star forming galaxies is indicated by the dashed green contours and its corresponding y-axis is shown on the right, where $Z=12+\log(\text{O/H})$. To guide the comparison of different distributions we show simple linear fits of the form $\log(\text{SFR})=a \times \log(L_{12\mu\text{m}})+b$ (dotted lines). Contours enclose 98%, 95%, 68% and 33% of the density distribution (68% for the case of strong AGN).

SFR/ M_{\odot} , that measures the current relative to past SFR needed to build up the stellar mass of the galaxy. The SSFR traces the star formation efficiency and its inverse defines the timescale for galaxy formation or the time the galaxy required to build up its current mass. Higher values of SSFR are indicative of a larger fraction of stars being formed recently. While ideally we would use gas mass or total mass instead of stellar mass for the normalization, such masses are not easily measured.

Figure 7 shows the SSFR as a function of $12 \mu\text{m}$ luminosity for the different galaxy classes. The nearly flat correlation for SF galaxies means that no matter the IR output, the amount of star formation per unit mass remains relatively constant. SF galaxies display a weak dependence with $L_{12\mu\text{m}}$ that gets narrower towards higher luminosities. As noted before, a possible origin for such residual SSFR could be due to a metallicity gradient. Calzetti et al. (2007) studied individual star forming regions of fixed aperture in nearby galaxies with known $\text{Pa}\alpha$ surface density, and found that low metallicity galaxies have a small deficit in $24 \mu\text{m}$ emission compared to high metallicity galaxies. Relaño et al. (2007) confirmed that while $24 \mu\text{m}$ luminosity is a good metallicity-independent tracer for the SFR of individual HII regions, the metallicity effect should be taken into account when analyzing SFRs integrated over the whole galaxy. We test qualitatively for a metallicity effect by calculating the SFR per unit mass per unit metallicity, where the metallicity is given by the $12+\log(\text{O/H})$ gas-phase oxygen abundance derived from optical nebular emission lines. The SF population displays an almost perfectly flat relationship over almost 4 orders of magnitude in $L_{12\mu\text{m}}$ such that independent of IR output, a galaxy of given mass and metal content converts gas into stars at a nearly constant rate. We note that these metallicities represent the current metal abundance rather than the luminosity-weighted average of past stellar populations. They also do not suffer from complications due to α -element enhancement or age uncertainties, characteristic of methods relying on absorption-line indices. Bond et al. (2011) arrive at a similar conclusion regarding a constant SSFR in nearby galaxies using Herschel $250 \mu\text{m}$ and WISE $3.4 \mu\text{m}$ data.

Compared to SF galaxies, AGN have SSFRs lower by a factor of ~ 10 , mainly because of their higher stellar masses. However, strong AGN lie much closer to the SF sequence than weak AGN. The former are hosted by high stellar mass galaxies, but also have young stellar populations that drive up the SFR at high $L_{12\mu\text{m}}$. Weak AGN do not have this boost in SFR and hence have lower SSFRs. Once again, composite systems populate a region intermediate between SF galaxies and strong AGN. Previous studies (e.g. Brinchmann et al. 2004; Salim et al. 2007) have shown the relationship between the SFR and M^* , identifying two different sequences: galaxies on a star-forming sequence and galaxies with little or no detectable SF. While the general result is that the SSFR of massive, red galaxies is lower at $0 < z < 3$, the exact dependence of SSFR on mass is still a matter of debate, particularly in view of recent results that trace the evolution at higher redshift (e.g. Noeske et al. 2007; Dunne et al. 2009; but see the discussion by Rodighiero et al. 2010). In our sample of SF galaxies we find that the dependence of $L_{12\mu\text{m}}$ on M^* is such that the efficiency by which gas is transformed into stars is nearly independent of the IR emission reprocessed by the dust. In strong AGN the star formation activity is “suppressed” moderately, but considerably more in the case of weak AGN. This suggests a sequence where a strong-AGN phase is a continuation of the SF sequence at high stellar mass, that gradually turns AGN into a population with weakened SF activity and lower $L_{12\mu\text{m}}$, dominated by older and redder stars.

Based on optical data, Kauffmann et al. (2003b) found that strong AGN hosts are indeed populated by relatively young stars, suggesting many of them could be post-starburst systems with extended star formation. With UV data, Salim et al. (2007) showed there is a close connection between massive SF galaxies and strong AGN. Using IR data, we find that the smooth sequence of galaxies from Figures 6 and 7 supports the hypothesis of strong AGN being the continuation at the massive-end of the normal SF sequence. An interesting question is whether the mid-IR luminosity in powerful AGN is driven by “normal” ongoing SF, or by hot dust left over *after* the last episode of SF. Further investigation is required to fully understand this matter.

3.7. SSFR Dependence on Mid-IR Color

Recent work on resolved nearby galaxies has shown a definite correlation between IR color and luminosity. Shi et al. (2011) found that for a variety of sources ranging from ULIRGs to blue compact dwarf galaxies, the flux ratio $f_{24\mu\text{m}}/f_{5.8\mu\text{m}}$ traces the SSFR and also correlates with the compactness of star forming regions. While ideally we would like to know the SFR surface density, we first explore the relation between SSFR and $4.6\text{--}12\mu\text{m}$ galaxy color, as shown in Figure 8. Galaxies from the main SF sequence (blue contours) correlate strongly with IR color, with strong AGN (black contours) continuing the trend at bluer colors. Weak AGN extend (red contours) that relationship remarkably well toward the low star formation end, albeit with higher dispersion and a slightly steeper slope. Hence, for the same increase in SSFR, AGN experience a smaller variation in IR color than typical SF objects. This is probably due to the combination of a metallicity effect and the different stel-

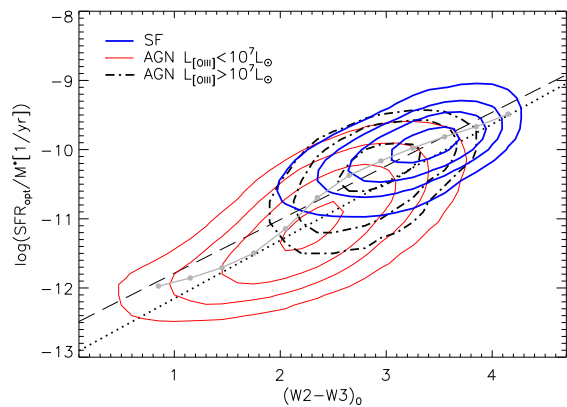


FIG. 8.— Specific star formation rate as a function of restframe $4.6\text{--}12\mu\text{m}$ galaxy color $(W2-W3)_0$ for SF galaxies (blue), strong AGN (dash-dot black) and weak AGN (red). The gray line indicates the median relation of the complete sample. The dashed and dotted lines correspond to linear fits to all sources and to all AGN, respectively. Contours enclose 95%, 85%, 68% and 33% of the density distribution (85%, 68% and 33% for the case of strong AGN).

lar populations that regulate the IR emission budget. In any case, this suggests that the higher the SSFR, the more prominent the $12\mu\text{m}$ IR emission becomes relative to $4.6\mu\text{m}$, where the latter is expected to strongly correlate with stellar mass. This shows that the $4.6\text{--}12\mu\text{m}$ color serves well as a rough first-order indicator of star formation activity over three orders of magnitude in SFR. A simple expression fitting all galaxies is given by

$$\log SSFR = (0.775 \pm 0.002)(W2-W3)_0 - (12.561 \pm 0.006). \quad (4)$$

If the galaxy is known to host an AGN, the more accurate expression is

$$\log SSFR = (0.840 \pm 0.008)(W2-W3)_0 - (12.991 \pm 0.020). \quad (5)$$

These results show that there is a tight link between stellar mass, current star formation rate and IR color in SF galaxies, which emphasizes the role of the dominant stellar population in regulating star formation.

3.8. Effect of AGN on the Energy Budget

In the previous sections we noted that the emission from the AGN could have a significant effect on the IR emission, and potentially bias the luminosities of the AGN galaxy class. This could be particularly important for low SFR galaxies. We test for this effect by estimating the contribution of the AGN to the total energy budget for sources classified from the BPT diagram as either an AGN or as an SF galaxy. To do so, we analyze the fraction of the $12\mu\text{m}$ luminosity contributed by each of the four templates used in the SED fitting process to our optical+IR photometry, paying particular attention to the AGN component. Figure 9 shows the median fraction of $12\mu\text{m}$ luminosity contributed by each template, for objects classified as SF galaxies. The majority of the power is split among the irregular (Im), spiral (Sbc) and elliptical (E) templates, though the AGN contribution becomes significant for the most luminous sources, above $10^{10.8}L_\odot$. This implies that the AGN has a negligible influence in SF galaxies. Figure 10 shows these fractions for weak and strong AGN galaxy classes. The elliptical component is now more prominent in weak AGN of

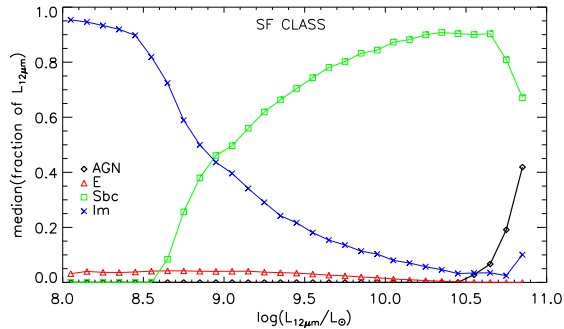


FIG. 9.— Median of the $12\ \mu\text{m}$ luminosity fraction contributed by the four templates from Assef et al. (2010) that are fitted to SDSS *ugriz* photometry and WISE $3.4\ \mu\text{m}$, $4.6\ \mu\text{m}$ and $12\ \mu\text{m}$ fluxes (we also use $22\ \mu\text{m}$ data when available). We include only objects classified as SF from the BPT diagram.

low luminosity, which is not unexpected. In general, the AGN component is now more important but is still far from contributing significantly below $10^{10.8}L_{\odot}$. In most weak AGN ($\sim 80\%$) the AGN contribution to the $12\ \mu\text{m}$ luminosity is below 40%. About $\sim 70\%$ of strong AGN show similar low AGN contributions at $12\ \mu\text{m}$. We note that in Figure 10 we used WISE aperture photometry for extended, nearby sources and profile-fitting magnitudes for unresolved galaxies with $\chi^2 < 3$ (see Section 4.5 of WISE Preliminary Release Explanatory Supplement for further details). Although the differences are small, aperture photometry improves the quality of the SED fit of low luminosity galaxies, as it captures the more extended flux of objects at low redshifts.

Note that in both cases, SF galaxies and AGN, the emission is dominated by the spiral (Sbc) component, which has a relatively high mid-IR SED. This is because the template, originally constructed by Coleman et al. (1980) and extended into the UV and IR with Bruzual & Charlot (2003) synthesis models, also considers emission in the mid-IR from dust and polycyclic aromatic hydrocarbons (PAHs). These are added by ad hoc linear combinations of appropriate parts of NGC 4429 and M82 SEDs obtained by Devriendt et al. (1999). Figure 11 shows the SED fit for AGN with luminosities of $L_{[\text{OIII}]} \sim 10^6 L_{\odot}$ and $L_{[\text{OIII}]} \sim 10^7 L_{\odot}$. In each case we plot the object with the median χ^2 , i.e. the typical fit for sources of those luminosities. The 9 photometric bands are well fitted by the model in most cases. For AGN with $L_{[\text{OIII}]} > 10^{7.5} L_{\odot}$ we find the SED fit is reasonably good (although in general with higher χ^2) except at the $22\ \mu\text{m}$ band. We believe this is caused by the limitation of the algorithm (not the templates themselves) to properly fit highly reddened AGN fainter than their hosts, as it is designed to punish the excessive use of reddening on the AGN when few relevant data points are used. Modifying the algorithm slightly to remove this behavior, we are able to obtain fits with better χ^2 values for these objects assigning much higher AGN fractions and reddening values, yet the lack of farther IR data to determine the origin of the $22\ \mu\text{m}$ excess makes these numbers also uncertain. Therefore, while these results do not definitely rule out that the central AGN could have a considerable effect in some extreme sources (e.g. the very strong AGN), it certainly shows that they are not relevant for most of the galaxy populations analyzed in this paper.

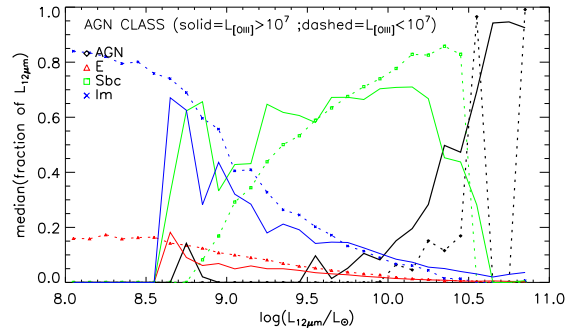


FIG. 10.— Same as Figure 9, but for objects classified as weak AGN (dashed) and strong AGN (solid).

4. SUMMARY

In this work we have taken advantage of recently released data from WISE and SDSS to construct the largest IR-optical sample of galaxies with $12\ \mu\text{m}$ fluxes and optical spectra available at $\langle z \rangle \sim 0.1$. This sample allowed us to investigate with high statistical significance how physical parameters such as color, stellar mass, metallicity, redshift, and SFR of $12\ \mu\text{m}$ -selected galaxies compare with purely optically selected samples. We have quantified how the SFR estimates compare for the different spectral types as a function of stellar mass, galaxy age and IR color in order to pinpoint the underlying source of $12\ \mu\text{m}$ emission and therefore up to what extent it could be interpreted as a useful SFR indicator.

The main results of this paper can be summarized as follows:

- In general, the WISE-SDSS $12\ \mu\text{m}$ -selected galaxy population traces the blue, late-type, low mass sequence of the bimodal galaxy distribution in the local Universe. It also traces intermediate-type objects with active nuclei, avoiding the bulk of the red and “dead” galaxies without emission lines. Most sources have normal to LIRG luminosities, but (few) ULIRGs are also present.
- The IR emission of SF galaxies and strong AGN, dominated by the blue, young stellar population component, is well correlated with the optical SFR. There is a small tendency of low SFR systems to have slightly lower IR luminosity when compared to the canonical relation of Chary & Elbaz (2001). These are low SFR, low mass systems that likely become more transparent due to the increasing fraction of light that escapes unabsorbed and hence suppresses $L_{12\ \mu\text{m}}$. However other effects like the dust distribution or metallicity could be relevant as well. The latter is shown by the (weak) SSFR dependence on $L_{12\ \mu\text{m}}$. In general, the mid-IR emission at $22\ \mu\text{m}$ follows similar correlations seen for the $12\ \mu\text{m}$ -selected sample, suggesting that these results do not critically depend on a single IR band.
- SF galaxies are forming stars at an approximately constant rate per unit mass for an IR output ranging over five orders of magnitude. There is small tendency for more luminous objects to have enhanced SSFR, which could be interpreted as a sign of SF histories peaking toward later times. However, this residual dependence seems to be caused

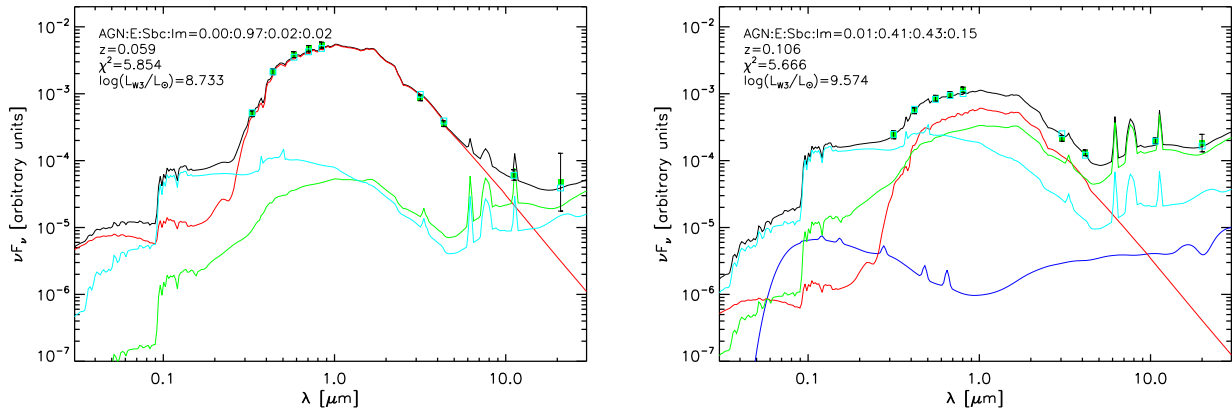


FIG. 11.— SED fits for AGN with the median χ^2 in two bins of $L_{[\text{OIII}]}$ centered at $L_{[\text{OIII}]} \sim 10^6 L_{\odot}$ (left) and $L_{[\text{OIII}]} \sim 10^7 L_{\odot}$ (right). The labels indicates the fraction of the bolometric luminosity contributed by each component template, which are shown in blue (AGN), red (E), green (Sbc), cyan (Im). The black line shows the total SED. The model SDSS and WISE photometry (cyan squares) are very similar to the observed photometric points (green squares).

by a metallicity gradient. Once factored out, the relationship becomes nearly flat. Strong AGN behave as a continuation at the massive-end of the normal SF sequence, where the AGN (possibly after a starburst episode) gradually quenches SF and weakens as it consumes the gas available, with the mid-IR emission fading in consequence.

- The mid-IR 4.6–12 μm restframe color can be used as a first-order indicator of the overall SF activity in a galaxy, as it correlates well with the specific SFR. For increasing SFR/ M^* , the IR emission becomes more prominent at 12 μm (associated with dust emission) relative to 4.6 μm (associated with stellar mass).
- For the case of SF galaxies, most of the mid-IR luminosity distribution is concentrated in systems younger than ~ 0.5 Gyr. Redder galaxies are dominated by older stellar populations, which contribute increasingly to the 12 μm emission. While many of these galaxies host an AGN (usually weak) the 12 μm energy budget is generally not dominated by the central active nuclei. This might not be the case of bright galaxies with very strong active nuclei ($L_{[\text{OIII}]} > 10^{7.5} L_{\odot}$) where a consid-

erably larger fraction of mid-IR emission could be due to the AGN. Spatially resolved, longer wavelength IR data and further modeling is necessary to fully understand these sources.

The authors thank G. Kauffmann, J. Brinchmann and S. Salim for useful suggestions. This publication makes use of data products from the Wide-field Infrared Survey Explorer, which is a joint project of the University of California, Los Angeles, and the Jet Propulsion Laboratory/California Institute of Technology, funded by the National Aeronautics and Space Administration. Funding for the SDSS and SDSS-II has been provided by the Alfred P. Sloan Foundation, the Participating Institutions, the National Science Foundation, the US Department of Energy, the National Aeronautics and Space Administration, the Japanese Monbukagakusho, the Max Planck Society and the Higher Education Funding Council for England. The SDSS Web Site is <http://www.sdss.org/>. R.J.A. was supported by an appointment to the NASA Postdoctoral Program at the Jet Propulsion Laboratory, administered by Oak Ridge Associated Universities through a contract with NASA.

REFERENCES

- Abazajian K. N. et al., 2009, *ApJS*, 182, 543
Alonso-Herrero A.; Ward M. J., Kotilainen J. K., 1997, *MNRAS*, 288, 977
Alonso-Herrero A., Rieke G. H., Rieke M. J., Colina L., Perez-Gonzalez P. G., Ryder S. D., 2006, *ApJ*, 650, 835
Assef R. J. et al., 2010, *ApJ*, 713, 970
Baldwin J., Phillips M., Terlevich R., 1981, *PASP*, 93, 5
Baldry I. K., Glazebrook K., Brinkmann J., Ivezić Z., Lupton R. H., Nichol R. C., Szalay A. S., 2004, *ApJ*, 600, 681
Blanton M. R., Roweis S., 2007, *AJ*, 133, 734
Bond N. A. et al., 2011, in preparation
Brinchmann J., Charlot S., White S. D. M., Tremonti C., Kauffmann G., Heckman T., Brinkmann J., 2004, *MNRAS*, 351, 1151
Bruzual G., Charlot S., 1993, *ApJ*, 405, 538
Bruzual G., Charlot S., 2003, *MNRAS*, 344, 1000
Calzetti D. et al. 2007, *ApJ*, 666, 870
Charlot S., Fall S. M., 2000, *ApJ*, 539, 718
Charlot S., Bruzual G., 2008, in preparation
Chary R., Elbaz D., 2001, *ApJ*, 556, 562
Coleman G. D., Wu C.-C., Weedman D. W., 1980, *ApJS*, 43, 393
Cutri R. et al., 2011, WISE Explanatory Supplement.
Daddi E. et al., 2007, *ApJ*, 670, 156
Devriendt J. E. G., Guiderdoni B., Sadat R., 1999, *A&A*, 350, 381
Duc P.-A. et al., 2002, *A&A*, 382, 60
Dunne L. et al., 2009, *MNRAS*, 394, 3
Eisenhardt P. et al., 2011, in preparation
Ferland G., 1996, Ferland G., 1996, *Hazy: A Brief Introduction to CLOUDY*. Internal Report, Univ. Kentucky
Griffith R. L. et al., 2011, *ApJ*, 736, 22
Heckman T. M., Robert C., Leitherer C., Garnett D. R., van der Rydt F., 1998, *ApJ*, 503, 646
Heckman, T. M., Kauffmann G., Brinchmann J., Charlot S., Tremonti C., White, S. D. M., 2004, *ApJ*, 613, 109
Hou L. G., Wu Xue-Bing, Han J. L., 2009, *ApJ*, 704, 794
Jannuzi B. et al., 2010, *Bulletin of the American Astronomical Society Meeting 215*, Vol 42., p.513
Jarrett T. et al., 2011, *ApJ*, 735, 112
Kauffmann G. et al., 2003a, *MNRAS*, 341, 33
Kauffmann G. et al., 2003b, *MNRAS*, 346, 1055
Keel W. C., De Grijp M. H. K., Miley G. K., Zheng W., 1994, *A&A*, 283, 791

- Kelson D. D., Holden B. P., 2010, *ApJL*, 713, 28
Kennicutt, R. C. Jr., 1998, *ARA&A*, 36, 189
Kennicutt, R. C. Jr. et al. 2009, *ApJ*, 703, 1672
Kochanek C. et al., 2011, in preparation
Lake S. E. et al., 2011, in preparation
Leisawitz D, Hauser M. G., 1988, *ApJ*, 332, 954
Martin D. C. et al., 2007, *ApJS*, 173, 342
Mulchaey J. S., Koratkar A., Ward M. J., Wilson A. J., Whittle M., Antonucci, R. R. J., Kinney A. L., Hurt T., 1994, *ApJ*, 436, 58
Neugebauer G. et al., 1984, *ApJ*, 278, 1
Noeske K. G. et al., 2007, *ApJ*, 660, L43
Rieke G. H., Alonso-Herrero A., Weiner B. J., Pérez-González P. G., Blaylock M., Donley J. L., Marcillac D., 2009, *ApJ*, 692, 556
Relaño M., Lisenfeld U., Pérez-González P. G., Vílchez J. M., Battaner, E., 2007, *ApJ*, 667, 141
Rocca-Volmerange B., de Lapparent V., Seymour N., Fioc M., 2007, *A&A*, 475, 801
Rodighiero G. et al., 2010, *A&A*, 518, 25
Saintonge A. et al., 2011, *MNRAS*, 415, 61
Salim S. et al., 2007, *ApJS*, 173, 267
Salim S. et al., 2009, *AJ*, 700, 161
Schlegel D. J., Finkbeiner D. P., Davis M., 1998, *AJ*, 500, 525
Seymour N., Rocca-Volmerange B., de Lapparent V., 2007, *A&A*, 475, 791
Shi Y. et al., 2011, in preparation
Shimasaku K. et al., 2001, *AJ*, 122, 1238
Skrutskie M.F. et al., 2006, *AJ*, 131, 1163
Soifer B. T. et al., 1987, *ApJ*, 320, 238
Spinoglio L., Malkan M. A., 1989, *AJ*, 342, 83
Stern D. et al., 2011, in preparation
Stoughton C. et al., 2002, *AJ*, 123, 485
Strateva I. et al., 2001, *AJ*, 122, 1861
Strauss M. A. et al., 2002, *AJ*, 124, 1810
Teplitz H. I. et al., 2011, *AJ*, 141, 1
Tremonti C. A. et al., 2004, *AJ*, 613, 898
Wright E. L. et al., 2010, *AJ*, 140, 1868
Wu H. et al., 2005, *ApJ*, 632, 79
Yan L. et al., 2011, in preparation
York D. G. et al., 2000, *AJ*, 120, 1579
Zhu Y. N., Wu H., Cao C., Li H.N., 2008, *ApJ*, 686, 155